# UNBINDING OF HYALURONAN ACCELERATES THE ENZYMATIC ACITIVITY OF BEE HYALURONIDASE

**Attila Iliás[1], Károly Liliom[2], Brigitte Greiderer-Kleinlercher[1], Stephan Reitinger[1] and Günter Lepperdinger[1]**

From Extracellular Matrix Research, Institute for Biomedical Aging Research, Austrian Academy of Sciences, Innsbruck, Austria[1] and Institute of Enzymology, Biological Research Center, Hungarian Academy of Sciences, Budapest, Hungary[2]

Running title: Unbinding site in bee hyaluronidase

Address correspondence to: Günter Lepperdinger, Extracellular Matrix Research, Institute for Biomedical Aging Research, Austrian Academy of Sciences, Rennweg 10, Innsbruck, A-6020, Austria. Tel: +43-512-583919-40 Fax: +43-512-583919-8

E-mail: guenter.lepperdinger@oeaw.ac.at

**Hyaluronan (HA), a polymeric glycosaminoglycan ubiquitously present in higher animals is hydrolyzed by hyaluronidases (HAases). Here we used bee HAase as a model enzyme to study HA-HAase interaction.**

**Located in close proximity to the active center, a bulky surface loop, which appears to obstruct one end of the substrate binding groove, was found to be functionally involved in HA turnover. To better apprehend kinetic changes in substrate interaction, binding of high molecular weight HA to catalytically inactive HAase was monitored by means of Quartz Crystal Microbalance technology. Replacement of the delimiting loop by a tetrapeptide interconnection increased the affinity for HA up to 100-fold, with a $K_D$ below 1 nM being the highest affinity amongst HA-binding proteins surveyed so far.**

**The experimental data of HA-HAase interaction were further validated showing best fit to the theoretically proposed sequential two-site model. Besides the one, which had been shown previously in course of X-ray structure determination, a previously unrecognized binding site works in conjunction with an unbinding loop that facilitates liberation of hydrolyzed HA.**

Hyaluronan (HA) is an unbranched glycosaminoglycan, which is composed of repeating disaccharide units of D-glucuronic acid and *N*-acetyl-D-glucosamine, and functional roles thereof are specifically related to its polymeric size (1). The shape and function of many anatomical structures in higher organism depend on high molecular weight HA as a ubiquitously present extracellular matrix determinant (2). Moreover, long HA chains also effectively modulate immune processes (3,4), while oligomeric HA stimulates angiogenesis (5), excites the synthesis of inflammatory cytokines (6), induces heat shock proteins and suppresses apoptosis (7). The respective polymeric size is thought to be the result of the balancing action of HA synthases (8) and hyaluronidases (HAase) (9,10), the latter being primarily responsible for HA degradation.

The HAase isolated from the venom gland of honey bee (bee venom HAase, or BVH) was the first HAase member of the endo-β-*N*-acetyl-hexosaminidase family (EC 3.2.1.35), to which also all human HAases belong, that could be molecularly cloned and recombinantly expressed (11). BVH is an endoglycolytic enzyme which catalyzes the hydrolysis of β-1,4 glycosidic bond of HA, as well as although with consistently lesser efficiency, chondroitin sulfates (12). In case of HA hydrolysis, the reducing end is generated at the terminal *N*-acetyl-D-glucosamine.

Many structural features of BVH are also present in human HAases such as HYAL1 (13) or HYAL2 (14). The 3-dimensional structure of BVH could be elucidated by means of X-ray crystallography (15). Moreover, the exact positioning of a HA tetramer tethered directly adjacent to the active center could be resolved. This data greatly argued for an acid/base catalytic mechanism, in which glutamic acid acts as the proton donor and the *N*-acetyl carbonyl group of the substrate as the nucleophilic base (16). The presence of an extended furrow spanning one hemisphere of the globular structure of the bee enzyme further suggested that long parts of the HA chain interact also with sites other than that next to the active centre.

In this study, we used BVH as a model enzyme, primarily because we could recently establish methods for high-yield recombinant expression in *Pichia pastoris* (12). We also wanted to investigate the function of a bulky structure delimiting one end of the putative substrate binding groove in acid-active HYAL-1, and as recently shown by us to be involved in regulating this enzyme's activity with respect to varying pH (17). Whether structural determinants in the close vicinity to this particular structure are actually involved in regulating substrate binding, or solely influence the active centre by long distance conformational changes remained elusive.

To address this question experimentally, we performed extensive kinetic analysis with wild-type recombinant BVH, as well as with a variant lacking the bulky formation. The results obtained suggest a likely role in substrate binding for the region next to the bulky formation. Working along this line we were able to reveal distinct kinetic parameters of substrate binding employing quartz crystal microbalance (QCM) technology (18,19). All results taken together, the presence of a second binding site could be demonstrated at that end of the substrate binding groove's opposite at the face of the bulky formation. This site probably controls product release.

## EXPERIMENTAL PROCEDURES

*Materials*

Hyaluronic acid potassium salt from human umbilical cord with an estimated average molecular mass of 750 kDa (H1504, lot 097K1495), chondroitin sulfate-A (27042, lot STBC0183V) with an estimated average molecular mass of 21 kDa (20,21), chondroitin sulfate-B (C3788, lot 080M1668V) of about 42 kDa (21), chondroitin sulfate-C (C4384, lot 1426300V) of about 60 kDa (22), N-acetyl-glucosamine (A8625), potassium tetraborate tetrahydrate (P5754), p-dimethyl-benzaldehyde (D2004) were purchased from Sigma.

*Molecular modeling*

The three dimensional structure of BVH has recently been deciphered in the presence of a HA tetrasaccharide by others (15). 3D-structural models of BVH isoforms and active centre variants were visualized using the open-source PyMol 1.1eval software (DeLano Scientific LLC) and further evaluated with the aid of the QMEAN method of SWISS-MODEL software (swissmodel.expasy.org) on the basis of coordinates for BVH in conjunction with a HA tetrasaccharide (PDB accession code, 1fcv) to validate the degree of nativeness of the BVH isoforms compared to the wildtype structure (23).

*Mutagenesis of hyaluronidase*

Numbering of the amino acids of BVH starts with Thr in its mature form (15). An inactive variant of BVH named NQ-BVH$^{WT}$ was obtained by mutation of both amino acids in the active centre, D111N and E113Q (24). The respective cDNAs were inserted into the yeast expression vector, pPIC9 in frame with the α-factor signal sequence and under the control of *AOX1* promoter using restriction sites *Eco*RI and *Not*I, respectively. Four-primer PCR technology was used to replace a 11-amino acid stretch, which loops out between the two cysteine residues at position 189 and 201 by the tetrapeptide GSGS. The mutagenesis primers were the following (the mutated nucleotides are underlined): forward 5'-TTCGCAGGAGCCACTACCGCAATAAGGGT AGGC-3' and reverse 5'-TATTGCGGTAGTGG CTCCTGCGAAGCGACCACC-3'. The resulting BVH variant was called BVH$^{\Delta L}$. This cDNA was further modified by replacement with the 5' terminal sequence of NQ-BVH$^{WT}$ using *Eco*RI and *Fse*I endonuclease yielding a cDNA encoding for the inactive isoform NQ-BVH$^{\Delta L}$. All sequences were validated by sequencing.

*Recombinant hyaluronidase expression and purification*

BVH variants were expressed in *Pichia pastoris*. The pPIC9 plasmid containing either wild-type or mutated cDNA was linearized by *Sal*I digestion and electrotransformed into GS115 strain. After methanol-induction of recombinant *Pichia* strains, high-yields of secreted BVH variants was found in the growth medium. The cells were removed by centrifugation, and the protein containing supernatant was filtered through a 0.45 μm filter and stored at -20°C for further use.

Ion exchange chromatography was performed as described previously (12) with minor modifications. Briefly, the supernatant was diluted with 3 volumes of 50 mM Na-acetate pH 5.0 and

applied onto a cation exchange column (5 ml HiTrap™ SP HP, GE Healthcare) in a cold room. The bound enzyme was eluted by 50% salt gradient of 2 M NaCl and subsequently the pooled fractions were desalted on 5 ml HiTrap™ Desalting columns (GE Healthcare).

*Measurement of enzymatic activity*

Generation of reducing ends through the action of HAase was determined based on the method established by Reissig (25). High molecular weight HA (5 mg/ml), or as a standard, N-acetyl-D-glucosamine were diluted to the desired concentration with 100 mM citrate buffer, pH 4.0 containing 137 mM NaCl and 2.7 mM KCl in a total volume of 100 µl. The mixtures were prepared on ice, and after pre-incubation at 37°C the reaction was started by adding enzyme (15 µg/ml of final concentration) diluted in the same buffer. The measurements were performed at 37°C and the reaction was stopped by heat inactivation (95°C, 3 min). Thereafter, 20% (v/v) of 0.8 M tetraborate solution was added and the samples were heated again at 95°C for 3 min. After chilling on ice, 5 volumes of acetic acid containing 1% (w/v) p-dimethyl-benzaldehyde and 0.375% (w/v) HCl were added and the samples were incubated at 37°C for 20 min. The optical density was measured by spectrophotometry at 585 nm. Four to six independent experiments were performed. One U of hyaluronidase activity is equal to the liberation of 100 nmol N-acetyl-D-glucosamine reducing ends generated by 1 mg enzyme.

Endoglycolytic cleavage within polymeric HA produces two products, and thus doubles the substrate concentration. Yet the number of β-1,4 glycolytic bonds available to the enzyme has actually decreased. Therefore, the number of cleavable β-1,4 linkages which also equals the number of disaccharide units of a polymeric HA chain was considered the basis for calculation of substrate concentration when building the kinetic model, also proposed previously elsewhere (26). Hence, the molar concentration of HA as a function of time is as follows:

$$[Ch]_t = A_1(1 - e^{-k_1 t}) + A_2(1 - e^{-k_2 t})$$

$k_1$ and $k_2$ are rate constants for degradation and $A_1$ and $A_2$ concentrations of specifically accessible β-1,4 HA bonds for cleavage. The initial reaction rates were calculated as the values of the first derivative of the two exponentials at time zero. The Michaelis-Menten kinetic parameters could be calculated by non-linear regression of the data using KaleidaGraph 4.1.1 (Synergy Software, USA).

*Quartz crystal microbalance measurements*

Carboxyl sensor chips were obtained from Attana AB (Stockholm, Sweden). The preparation of the sensor chips and the immobilization procedure by amine coupling were performed according to the manufacturer's instructions. Briefly, a carboxyl chip was pre-wetted with MilliQ water prior to the immobilization and was inserted in the Attana A100 QCM biosensor instrument (Attana AB, Stockholm, Sweden), and left to stabilize. The immobilization procedure was carried out at a flow rate of 10 µl/min in HBS-T buffer (10 mM HEPES, 150 mM NaCl, 0.005% Tween 20, pH 7.4) at 25°C. Thereafter, 0.4 mM EDC and 0.1 mM Sulfo-NHS were mixed in 1:1 ratio and the solution was injected immediately with 300 sec of contact time in order to activate the chip surface. After rinsing the injection loop with MilliQ water the ligand solution containing 20 or 10 µg/ml of purified NQ-BVH$^{WT}$ and NQ-BVH$^{\Delta L}$, respectively, in 10 mM Na-acetate buffer, pH 5.0, was loaded to the chip for 300 sec. The injection loop was washed again with MilliQ water, and finally, the remaining activated carboxyl groups on the chip surface were neutralized by the injection of 1 M ethanolamine, pH 8.5 for 300 sec. For detecting background responses, a chip without protein was prepared following the same procedure. Substrate binding experiments were performed with a continuous flow (25 µl/min) of running buffer (20 mM citrate buffer, 137 mM NaCl, 2.7 mM KCl, 0.005% Tween 20, pH 4.0) allowing for a contact time of 100 sec. Substrate samples were prepared by serial dilutions in running buffer and the interaction was recorded with the aid of Attester® software (Attana AB, Stockholm, Sweden) for HA concentrations ranging from 0.05 to 1.0 mg/ml and for chondroitin sulfate concentrations ranging from 0.05 to 0.5 mg/ml injected in a random order at 37°C. After each measurement the chip surface was regenerated by a 30 sec injection of 2 M NaCl to remove any remaining analyte. Two to three independent experiments were performed.

The frequency response curves of the interaction between the various substrates at different concentrations and the immobilized inactive BVH variants, as well as the unmodified surface were analyzed by the Attache Evaluation software, version 3.3.3.1 (Attana AB, Stockholm, Sweden). The curves obtained at distinct substrate concentrations were averaged and corrected by subtracting the non-specific binding responses obtained from measurements using unmodified surface. The kinetic data analysis was performed using ClampXP2 3.50 provided by the developers (27), by fitting theoretical models to the experimental data. First, a global analysis attempt was made, which proved insufficient. Next, a local analysis of the association and the dissociation phases was performed. The equilibrium dissociation constants of BVH variants for high molecular weight HA and chondroitin sulfates were calculated from the directly estimated association and dissociation rate constants ($K_D=k_{diss}/k_{ass}$).

## RESULTS

*Enzyme activity and kinetic analysis*

The substrate binding groove of HAase is constrained at one end by a bulky noose, which comprises a short stretch of amino acids that loop out at a cystine bridge linking position 189 and 201. By means of computer-aided homology modeling (23), this loop could be replaced by the tetrapeptide GSGS, which yielded the enzyme variant $BVH^{\Delta L}$ (Figure 1A). When expressed in *Pichia pastoris*, both the wild-type and the mutant form were secreted into the growth medium, from where large quantities of active enzyme could be purified (Figure 1B). Compared to wild-type, $BVH^{\Delta L}$ exhibited lower specific activity, and although both HAases were active throughout a wide pH range, $BVH^{\Delta L}$ was found inactive above pH 7.0. For subsequent substrate binding studies, also inactive isoforms of both $BVH^{WT}$ and $BVH^{\Delta L}$ were generated by substituting the two essential acidic residues of the active centre. The resulting mutants D111N/E113Q-$BVH^{WT}$ and D111N/E113Q-$BVH^{\Delta L}$ were named NQ-$BVH^{WT}$ and NQ-$BVH^{\Delta L}$; both mutant isoforms lacked any detectable HAase activity (data not shown).

Turnover rates were assessed by monitoring the formation of reducing ends during HA depolymerization. As both $BVH^{WT}$ and $BVH^{\Delta L}$ exhibited highest activities between pH 3.0 and pH 5.5 (Figure 1B), kinetic analyses were performed at pH 4.0. Both variants showed a progressive decrease of reaction rates at substrate concentrations up to 2 mg/ml. The best fit for all series of experimental data points was a biexponential function, displaying two distinct phases of a putative two-step process: during the early phase, the number of reducing ends increases rapidly, high molecular weight HA is efficiently hydrolyzed and a large amount of oligomeric substrate is generated; thereafter reaction rates gradually decrease. Even in the presence of high HA concentrations, $BVH^{WT}$ could always reach this late phase. In contrast, $BVH^{\Delta L}$ showed reduced hydrolysis rates during the early stage, and kinetics only approached the late phase during the time-course of the experiment at low HA concentrations (Figure 2).

Next, the initial reaction rates were calculated and plotted against HA concentration. The kinetic curves clearly showed that hydrolysis rates gradually decreased at HA concentration higher than 0.5 mg/ml for $BVH^{WT}$, or 0.2 mg/ml for $BVH^{\Delta L}$. Consequently, the initial reaction rates showed asymmetric, bell-shaped concentration dependencies with optima between 0.2-0.5 mg/ml HA for the wild-type enzyme (Figure 3A). Despite displaying similar characteristics, the initial rate of $BVH^{\Delta L}$ was found to be 10-times lower (Figure 3B).

The biexponential progression of HA hydrolysis could be resolved into two kinetic phases: a dominant fast-rate step ($v_0 1$) and a slow process with a distinctly lower rate ($v_0 2$). Both the wild-type and the mutant enzyme have comparable $v_0 2$; the 10-fold difference in $v_0$ is largely due to a rate difference of the dominant reaction $v_0 1$ (Figure 3). At the early phase of the reaction solely high molecular weight HA is present, which is degraded by the wild-type enzyme with high $v_0 1$. This suggests that the turnover rate of long chains appears to be enhanced through the action of the bulky loop, be it through long-distance conformational changes of the active centre or modulated through influencing substrate binding.

Next, $V_{max}$ and $K_m$ of the hydrolysis reaction were estimated by performing curve fitting of the ascending and descending phases of the initial rate progress. The $V_{max}$ for $BVH^{WT}$ was $1 \cdot 10^6 \pm 3 \cdot 10^4$,

and that of BVH$^{\Delta L}$ converged to $1.3 \cdot 10^5 \pm 2 \cdot 10^3$ U/min. Unexpectedly, BVH$^{\Delta L}$ had a lower $K_m$ compared to BVH$^{WT}$ (0.24 ± 0.01 vs. 0.37 ± 0.08 mg/ml), indicative for higher substrate affinity.

*Substrate binding*

Under the experimental conditions used in the previous kinetic analyses, substrate degradation rates of BVH and the loop variant were too high for binding studies. Therefore, interactions at varying HA concentrations (0.05 – 1 mg/ml) were studied with the inactive HAase variants NQ-BVH$^{WT}$ and NQ-BVH$^{\Delta L}$. Both HAase variants firmly bound high molecular weight HA. The point mutations introduced in the active centre, although located within the substrate binding groove did not induce major conformational changes, which incommode HA binding. Moreover, the polymer could be detached from both variants. Prior to a successive measurement the chip was efficiently regenerated by washes with high ionic strength buffer (Figure 4).

Working along these lines experimental data for HA association to and dissociation from the inactive HAase variants were collected. The results obtained thereby were further validated using previously established theoretical models. A fit to the simple Langmuir binding model could not be accomplished, both the simple binding, as well as the mass transport-limited models were unable to adequately describe the interaction. This suggested that interactions between HA and BVH are more complex. Therefore various two-state models were challenged (28-30) and finally, a two-site model was computed, which provided useful fits. When supposing substrate binding in random order the estimation of two out of four association rate constants ($k_{ass}$) yielded no meaningful results, suggesting that distinct binding events are either negligible or random combinations of binding and unbinding are likely circumstantial. Challenging the alternative proposition that binding may take place in a directed fashion the following sequential two-site model was fitted:

$$S1 + HA \rightleftharpoons S1.HA + S2 \rightleftharpoons S1.HA.S2$$

$S1$ and $S2$ are putative substrate binding sites, and thus this model assumed that the enzyme actually accommodates two distinct binding sites, which associate with the polymer in a sequential order. Also, this particular model approximated the experimental data regarding the interaction of HA with the two inactive variants best, as the kinetics showed congruent matches for all experimental data sets (Figure 4). Since the global fitting algorithm could not be applied, the association ($k_{ass}$) and dissociation ($k_{diss}$) constants, as well as the equilibrium dissociation constants ($K_D$) were determined for each HA concentration by local fitting (Table 1).

When plotting $k_{ass}$ and $k_{diss}$ rate constants of the two binding sites against substrate concentration, it became apparent that when comparing the derived data to that of the wild-type enzyme, the inactive loop variant, NQ-BVH$^{\Delta L}$ formed the HA-enzyme complex at a considerably higher rate as reflected by a higher $k_{ass,}$ at the second binding site. Moreover, HA was released more slowly from the complex as $k_{diss}$ at the second binding site was distinctly lower. In either variant, $k_{ass}$ and $k_{diss}$ of the first binding site were found comparable thus indicating that the putative second binding site is locally close to the bulky loop (Figure 5A and B). Also line-up of the $K_D$s regarding the first binding sites ($K_{D1}$) showed highly similar results for both variants, with a sole exception of a slight difference at the highest experimental HA concentration. In the case of NQ-BVH$^{\Delta L}$, the second binding site exhibited again a significantly lower $K_{D2}$ (Figure 5C), by and large confirming the aforementioned assumption that the bulky formation solely impinges on the putative second binding site, which when not affected by the loop has high HA affinity.

Furthermore, comparison of the overall affinity constants ($K_{DSUM}$) as calculated from the $K_D$ values of both binding site ($K_{D1}$*$K_{D2}$), revealed the highest value for the wild-type protein with 62.9 nM at 0.5 mg/ml HA, whereas the loop variant exhibited 10 to 100-times lower $K_D$ values with a maximum value of 0.98 nM at 0.2 mg/ml HA concentration (Table 1). Thus, replacement of the bulky formation greatly enhanced the enzyme's overall affinity for high molecular weight HA yielding tight binding and/or impeded product release.

Chondroitin sulfate (CS) A, B, and C are also substrates to BVH. Compared to HA, the hydrolysis rate of CS-C is approximately 40%, for CS-C 20%, and CS-B is only very slowly

degraded (12). Binding of all three CS types to NQ-BVH$^{WT}$, as well as to NQ-BVH$^{\Delta L}$ was evaluated accordingly (Supplemental Figures 1-6,). Analysis of $K_{DSUM}$ for the CS types with regard to HA showed that substrate binding is an important actuating value determining turnover rates (Supplemental Table 1-3), as CS-B showed the highest $K_{DSUM}$ value of 801 nM at 0.5 mg/ml for the wild-type and 257 nM at 0.2 mg/ml for the loop variant (Supplemental Table 2), and CS-A and CS-C showed $K_{DSUM}$ values of 172 nM at 0.5 mg/ml and 198 nM at 0.05 mg/ml for NQ-BVH$^{WT}$, and 42.5 nM at 0.2 mg/ml and 19 nM at 0.1 mg/ml for NQ-BVH$^{\Delta L}$, respectively. Further kinetic analyses showed best fit of the respective data again to the sequential two-site model.

In view of these results we here propose a model for the cleavage cycle of HAase featuring two distinct binding sites, which sequentially bind and release the products accordingly (Figure 6).

## DISCUSSION

The published crystal structures of HAases from bee (15) and wasp venom (31), or that of human serum HAase, HYAL-1 (32) led to the identification of a bulky knob, which rises at the upper end of the substrate binding groove. Both length and amino acid composition of this unshaped bump are highly variable, with the sole exception of a single asparagine residue which is conserved in most species. In many hyaluronidases from hymenoptera, that asparagine is part of a potential N-glycosylation recognition sequence, which in all cases characterized so far is followed by a proline. This combination however renders this particular site highly unlikely for posttranslational glycosylation (33). This assumption was further strengthened by comparing wild-type BVH with BVH$^{\Delta L}$ in which the respective stretch had been replaced with a tetrapeptide sequence comprising alternating Gly and Ser residues. The latter thus lacks the potential glycosylation site. After expression in *Pichia pastoris*, a microbe known to efficiently glycosylate, the molecular weight of the two secreted proteins was found comparable. Interestingly, enzymatic and kinetic analyses of BVH$^{\Delta L}$ in which the blocking knob has been depleted showed that it has reduced activities.

Previous analyses with bovine testicular hyaluronidase had shown that two phases of HA hydrolysis can be distinguished: an early part, where high-molecular-weight HA was found to be degraded at a relatively fast rate; thereafter the resulting oligomeric fragments were hydrolyzed with slow kinetics (26,34,35). This was found to be true for wild-type BVH activity. However, the results obtained for BVH$^{\Delta L}$ which supposedly should offer more open space for a high molecular weight substrate, were unexpected. The rapid early phase of HA hydrolysis was not found for the enzyme variant. Although counterintuitive, this bulky loop actually enhances turnover of polymeric HA.

The initial reaction rates for both wild-type and BVH$^{\Delta L}$ clearly showed an inhibition at high HA concentration. As previously reported, short HA fragments are poor substrates for HAases (34,35). Provided that the atypical bell-shaped progression of the substrate concentration dependence could be due to increasing amounts of short HA oligomers in concentrated polydispers substrate solutions. Increasing concentrations of short HA may thus shift to late phase kinetics and greatly decelerate the overall turnover rate. It is, however, also conceivable that similar to steric exclusion of bovine serum albumin in highly concentrated HA solutions (36,37) the observed suppression of enzyme activity could also be a consequence of crowding out of HAase by closely interacting HA chains.

To address this open question, the kinetic data sets were analyzed further. Working along these lines yet only yielded the approximation of Michaelis-Menten parameters. Still acceptable estimates for $V_{max}$ and $K_m$ could be achieved. An important result was that $K_m$ for BVH$^{\Delta L}$ was found to be much lower, thus indicating enhanced affinity for HA.

More detailed binding studies were performed by means of QCM technology, which is capable of monitoring the interaction in real-time as a change in frequency of a surface coated quartz crystal resonator. In solution this method is highly effective at determining the affinity of molecules, in particular for large binding partners, such as high molecular weight HA. So far no experimental results based on QCM were available for HA-HAase interaction. Surface Plasmon Resonance has previously been introduced to monitor the

interactions of bovine testicular hyaluronidase with sulfated glucosaminoglycans. Notably, however, HA as the major binding partner for HAase has for unknown reasons not been studied (38).

When using enzymatically active HAase in QCM measurements, binding could be examined, but due to hydrolysis taking place at the same time with concomitant generation of highly polydispers HA, no distinct models for subsequent data analysis could be built. Stable interaction of HA, and other substrates such as CS with the enzyme could only be studied for HAase lacking hydrolysis activity. Mutations of specific catalytic residues in the active center were previously reported to inactivate human testicular hyaluronidase (24), as well as HYAL-1 (39). Point mutations introduced into BVH also yielded an inactive variant, which still bound high molecular weight substrate efficiently. From data obtained with this variant, a sequential two-site model could be deduced that features a dynamic mechanism involving a second potential binding site, which only becomes available after a first site has been successfully occupied by an uncleaved polymeric substrate. According to this model we propose the existence of two kinetically distinct binding sites, which are both located in the substrate binding groove on either side of the active center. Following the nomenclature for sugar binding sites in glycosyl hydrolases (40), the first binding site (S1) is at the –n subsites away from the non-reducing end of cleaved HA, while the second binding site (S2), which we mapped next to the bulky formation interacts with HA at +n subsites, with cleavage taking place in between -1 and +1.

The model of the cleavage cycle as depicted in Figure 6 states that initial attachment at S1 is mandatory for HA in order to subsequently interact with S2. After completion of the hydrolytic reaction the HA-fragment bound to S2 will be released first and only thereafter the remaining fragment detaches from S1. Replacement of the loop yielded a variant with lower enzymatic activity but with up to 100-times higher affinity in HA-binding. The equilibrium dissociation constant, $K_D$ for high molecular weight HA was found to be 0.05 to 0.98 nM, while the $K_D$ for the wild-type enzyme was only 1.77 to 62.9 nM. Previously reported $K_D$ for HA-binding proteins or hyalectins were 5-150 μM for CD44 (41-43), 11-36 μM for LYVE-1 (43), 0.2-55 μM for TSG-6 (44,45), 226 nM for aggrecan and exactly 82 nM for Link protein (46). The HA receptor for endocytosis, HARE has the highest affinity for HA ranging 5 to 23 nM (47,48). Compared to these specific binding proteins, the BVH loop variant shows the highest avidity for HA.

Indeed, the bulky formation interferes with HA binding, but probably promotes the unbinding of short oligomeric chains tethered to the +n site. The penultimate step of the catalytic cycle had actually been depicted before by X-ray structure determination of BVH co-crystallized with a HA-hexasaccharide. In the crystals, the HA-hexasaccharide had been degraded, and the HAase only retained a tetrasaccharide fragment bound to the subsites -4 to -1. At the –n subsites amino acids, which directly interact with HA such as Tyr55, Asp111, Glu113, Tyr184, Tyr227, Trp301, Ser303 and Ser304 could be identified (15). In turn, however, the situation regarding the +n subsites was less clear. To gain more insight, the 3D coordinates of HA derived from the crystal structure of the BVH-HA complex were used for computational modeling studies placing a virtual HA chain all along into the binding groove of HYAL1. In this way amino acid residues located as close as 5 Å to the HA molecule could be identified. These were Asp129, Glu131, Tyr202, Tyr247, Ser245 and Arg265 (39). The latter two correspond to Ser225 and Arg244 of the bee enzyme. However, no direct interaction with the HA-tetrasaccharide had been reported in the previous study (15). Also in close vicinity to the bulky knob, Ser225 and Arg244 are likely residues of the +n subsites, and thus shaping the second binding site.

In conclusion, we report here that the bulky formation, which at the first glance appears to block the substrate binding groove, actually contributes to a second HA binding site in HAase. The results presented in this study demonstrate that this loop is involved in modulation of the enzymatic activity, which besides substrate binding also requires efficient clearing of the products after catalytic processing. In turn, when a product is transiently retained at the second site through strong binding, further progression through the catalytic cycle is retarded. Through the bulky loop in BVH release of the cleaved HA

fragment from the enzyme is increased which results in a higher rate of hydrolysis.

The various bulky formations in different hyaluronidase species may have evolved to efficiently hydrolyze high molecular weight HA in different biological processes. The bee venom enzyme is considered to be a spreading factor. At the site of a bee sting, rapid hydrolysis of HA chains in the dermis facilitates the diffusion of other venom constituents, mainly the lytic peptide mellitin and phospholipase, thereby augmenting local damage and inflammation.

**Acknowledgments:** The authors would like to thank Günther Kreil for careful reading of the manuscript and fruitful discussions. GL is supported by research funds granted by the Austrian Research Agency FFG, the Tyrolean Future Fund and the EC's 7th framework program. SR is recipient of a Marie-Curie International Re-Integrations grant.

**REFERENCES**

1. Hascall, V., and Esko, J. D. (2009) Hyaluronan. in *Essentials of Glycobiology* (Varki, A., Cummings, R. D., Esko, J. D., Freeze, H. H., Stanley, S., Bertozzi, C. R., Hart, G. W., and Etzler, M. E. eds.), 2010/03/20 Ed., Cold Spring Habor Laboratory Press, Cold Spring Habor. pp
2. Wang, A., de la Motte, C., Lauer, M., and Hascall, V. (2011) *FEBS J* **278**, 1412-1418
3. Jiang, D., Liang, J., and Noble, P. W. (2011) *Physiol Rev* **91**, 221-264
4. Delmage, J. M., Powars, D. R., Jaynes, P. K., and Allerton, S. E. (1986) *Ann Clin Lab Sci* **16**, 303-310
5. West, D. C., Hampson, I. N., Arnold, F., and Kumar, S. (1985) *Science* **228**, 1324-1326
6. Noble, P. W. (2002) *Matrix Biol* **21**, 25-29
7. Xu, H., Ito, T., Tawada, A., Maeda, H., Yamanokuchi, H., Isahara, K., Yoshida, K., Uchiyama, Y., and Asari, A. (2002) *J Biol Chem* **277**, 17308-17314
8. Tammi, R. H., Passi, A. G., Rilla, K., Karousou, E., Vigetti, D., Makkonen, K., and Tammi, M. I. (2011) *FEBS J* **278**, 1419-1428
9. Stern, R. (2003) *Glycobiology* **13**, 105R-115R
10. Stern, R., Asari, A. A., and Sugahara, K. N. (2006) *Eur J Cell Biol* **85**, 699-715
11. Gmachl, M., and Kreil, G. (1993) *Proc Natl Acad Sci U S A* **90**, 3569-3573
12. Reitinger, S., Boroviak, T., Laschober, G. T., Fehrer, C., Mullegger, J., Lindner, H., and Lepperdinger, G. (2008) *Protein Expr Purif* **57**, 226-233
13. Frost, G. I., Csoka, A. B., Wong, T., and Stern, R. (1997) *Biochem Biophys Res Commun* **236**, 10-15
14. Lepperdinger, G., Strobl, B., and Kreil, G. (1998) *J Biol Chem* **273**, 22466-22470
15. Markovic-Housley, Z., Miglierini, G., Soldatova, L., Rizkallah, P. J., Muller, U., and Schirmer, T. (2000) *Structure* **8**, 1025-1035
16. Markovic-Housley, Z., and Schirmer, T. (eds). (2002) *Structural evidence for substrate assisted catalytic mechanism of bee venom hyaluronidase, a major alergen of bee venom*, The Royal Soc Chemistry, MPG Books Ltd, Bodmin Cornwall UK
17. Reitinger, S., Mullegger, J., Greiderer, B., Nielsen, J. E., and Lepperdinger, G. (2009) *J Biol Chem* **284**, 19173-19177
18. Sauerbrey, G. (1959) *Zeitschrift für Physik* **155**, 206-222
19. Bruckenstein, S., and Shay, M. (1985) *Electrochim Acta* **30**, 1295-1300
20. Jumel, K., Harding, S. E., Sobol, E., Omel'chenko, A., Sviridov, A., and Jones, N. (2002) *Carbohyd Polym* **48**, 241-245
21. Hess, R., Douglas, T., Myers, K. A., Rentsch, B., Rentsch, C., Worch, H., Shrive, N. G., Hart, D. A., and Scharnweber, D. (2010) *J Biomech Eng* **132**, 021001
22. Rees, S. G., Shellis, R. P., and Embery, G. (2002) *Biochem Biophys Res Commun* **292**, 727-733
23. Benkert, P., Biasini, M., and Schwede, T. (2011) *Bioinformatics* **27**, 343-350
24. Arming, S., Strobl, B., Wechselberger, C., and Kreil, G. (1997) *Eur J Biochem* **247**, 810-814

25. Reissig, J. L., Storminger, J. L., and Leloir, L. F. (1955) *J Biol Chem* **217**, 959-966
26. Vincent, J. C., Asteriou, T., and Deschrevel, B. (2003) *J Biol Phys Chem* **3**, 35-45
27. Myszka, D. G., and Morton, T. A. (1998) *Trends Biochem Sci* **23**, 149-150
28. Morton, T. A., Myszka, D. G., and Chaiken, I. M. (1995) *Anal Biochem* **227**, 176-185
29. Karlsson, R., and Falt, A. (1997) *J Immunol Methods* **200**, 121-133
30. De Crescenzo, G., Grothe, S., Lortie, R., Debanne, M. T., and O'Connor-McCourt, M. (2000) *Biochemistry* **39**, 9466-9476
31. Skov, L. K., Seppala, U., Coen, J. J., Crickmore, N., King, T. P., Monsalve, R., Kastrup, J. S., Spangfort, M. D., and Gajhede, M. (2006) *Acta Crystallogr D Biol Crystallogr* **62**, 595-604
32. Chao, K. L., Muthukumar, L., and Herzberg, O. (2007) *Biochemistry* **46**, 6911-6920
33. Gavel, Y., and von Heijne, G. (1990) *Protein Eng* **3**, 433-442
34. Deschrevel, B., Tranchepain, F., and Vincent, J. C. (2008) *Matrix Biol* **27**, 475-486
35. Cramer, J. A., Bailey, L. C., Bailey, C. A., and Miller, R. T. (1994) *Biochim Biophys Acta* **1200**, 315-321
36. Ogston, A. G., and Preston, B. N. (1966) *J Biol Chem* **241**, 17-19
37. Shaw, M., and Schy, A. (1977) *Biophys J* **17**, 47-55
38. Shen, B., Shimmon, S., Smith, M. M., and Ghosh, P. (2003) *J Pharm Biomed Anal* **31**, 83-93
39. Zhang, L., Bharadwaj, A. G., Casper, A., Barkley, J., Barycki, J. J., and Simpson, M. A. (2009) *J Biol Chem* **284**, 9433-9442
40. Davies, G. J., Wilson, K. S., and Henrissat, B. (1997) *Biochem J* **321**, 557-559
41. Skelton, T. P., Zeng, C., Nocks, A., and Stamenkovic, I. (1998) *J Cell Biol* **140**, 431-446
42. Banerji, S., Noble, M., Teriete, P., Wright, A. J., Blundell, C. D., Campbell, I. D., Day, A. J., and Jackson, D. G. (eds). (2005) *Structure of the CD44 hyaluronan-binding domain and insight into its regulation by N-glycosylation*, Vol. II, pp. 625-630, Matrix Biology Institute, Edgewater, NJ
43. Banerji, S., Hide, B. R., James, J. R., Noble, M. E., and Jackson, D. G. (2010) *J Biol Chem* **285**, 10724-10735
44. Kohda, D., Morton, C. J., Parkar, A. A., Hatanaka, H., Inagaki, F. M., Campbell, I. D., and Day, A. J. (1996) *Cell* **86**, 767-775
45. Kahmann, J. D., O'Brien, R., Werner, J. M., Heinegard, D., Ladbury, J. E., Campbell, I. D., and Day, A. J. (2000) *Structure* **8**, 763-774
46. Watanabe, H., Cheung, S. C., Itano, N., Kimata, K., and Yamada, Y. (1997) *J Biol Chem* **272**, 28057-28065
47. Harris, E. N., Kyosseva, S. V., Weigel, J. A., and Weigel, P. H. (2007) *J Biol Chem* **282**, 2785-2797
48. Harris, E. N., Parry, S., Sutton-Smith, M., Pandey, M. S., Panico, M., Morris, H. R., Haslam, S. M., Dell, A., and Weigel, P. H. (2010) *Glycobiology* **20**, 991-1001
49. Varki, A., Cummings, R. D., Esko, J. D., Freeze, H. H., Stanley, P., Marth, J. D., Bertozzi, C. R., Hart, G. W., and Etzler, M. E. (2009) *Proteomics* **9**, 5398-5399

## FOOTNOTES

The used abbreviations are: HA, hyaluronan; CS-A, chondroitin sulfate-A; CS-B, chondroitin sulfate-B; CS-C, chondroitin sulfate-C; BVH, bee venom hyaluronidase; HYAL-1, human serum hyaluronidase 1; QCM, Quartz Crystal Microbalance; PDB, protein database; AOX1, alcohol oxidase 1

## FIGURE LEGENDS

FIGURE 1: **3D-models and enzymatic activity of the wild-type and the loop mutant of bee hyaluronidase**
The steric models of $BVH^{WT}$ (left) and $BVH^{\Delta L}$ (right) with a bound HA-tetrasaccharide (blue in stick mode) were generated using PyMol. The wild-type and the mutant loops are highlighted in yellow and

green, respectively, and the active centers, D111 and E113 are shown in magenta and red, respectively (*Panel A*). Expression of the wild-type enzyme and the variant were analyzed on a 12% SDS-PAGE and visualized by Coomassie-staining. The arrow indicates the expected molecular masses (*inset in Panel B*). Determination of pH dependence of $BVH^{WT}$ (● and solid line), and $BVH^{\Delta L}$ (■ and dashed line) using 0.1 mg/ml of HA concentration and 20 min of incubation time at 37°C was performed by Reissig assay (n=3). The values represent the mean ± S.E. and in 80% of all data sets S.E. were <10%. The enzyme activity is expressed in Units (U), 1 Unit equaling 0.1 nmol of reducing N-acetyl-D-glucosamine end groups generated by 1 mg of enzyme (*Panel B*).

FIGURE 2: **Kinetics of HA hydrolysis at different substrate concentrations**
The time-course of HA hydrolysis of $BVH^{WT}$ (*Panel A*) and $BVH^{\Delta L}$ (*Panel B*) was detected by Reissig assay at pH 4.0 and at 0.05 (● and solid line), 0.1 (■ and dashed line), 0.2 (♦ and dotted line), 0.5 (▲ and solid line), 0.8 (▼ and dashed line), 1.0 (● and dotted line), 1.2 (■ and solid line) and 2.0 mg/ml (♦ and dashed line) of HA concentration at 37°C (n=4-6). The enzyme activity is expressed in Units (U). The values represent the mean ± S.E. and in 90% of all data sets S.E. were <15%.

FIGURE 3: **Substrate dependence of HA hydrolysis**
Initial reaction rates of $BVH^{WT}$ (● and solid line) *on Panel A* and $BVH^{\Delta L}$ (■ and dashed line) *on Panel B* at different HA concentrations were calculated from the biexponential parameters derived from the time-course measurement. Decomposing the kinetic phases yielded a fast-rate reaction ($v_0 1$, ▲ and dotted line) and a slow process ($v_0 2$, ♦ and dotted line). The substrate progress curves were obtained by fitting the superposition of a saturated with an analogous displacement function.

FIGURE 4: **QCM sensorgrams for substrate binding**
Inactive forms of BVH containing the normal (*Panel A*) and the mutated loop sequences (*Panel B*) were used for QCM measurements. Varying HA concentrations (0.05 to 1.0 mg/ml) were loaded onto immobilized BVH in a random order and interactions were monitored at pH 4.0 and at 37°C (solid lines) (n=2-3). The curves from each HA concentrations were averaged and corrected by subtracting the non-specific binding responses obtained from the unfunctionalized surface. The sequential two-site model was fitted (dotted lines) to the averaged sensorgrams by local analysis using ClampXP2 software.

FIGURE 5: **Comparison of the association and dissociation rate constants of HA-binding**
The association ($k_{ass}$) (*Panel A*) and the dissociation rate constants ($k_{diss}$) (*Panel B*) of the first (● and dotted line) and the second binding sites (● and solid line) of NQ-$BVH^{WT}$ and the first (■ and dotted line) and the second binding sites (■ and solid line) of NQ-$BVH^{\Delta L}$ were estimated directly during the fitting procedure. The $K_D$ values of the first (● and dotted line) and the second binding sites (● and solid line) of NQ-$BVH^{WT}$ and the first (■ and dotted line) and the second binding sites (■ and solid line) of NQ-$BVH^{\Delta L}$ were calculated from the association and the dissociation constants ($K_D = k_{diss}/k_{ass}$) (*Panel C*). Values represent the mean ± S.E. and in 78% of all data sets S.E. were <25%.

FIGURE 6: **Cleavage cycle of bee hyaluronidase**
The schematic representation of the model for the cleavage cycle was built-up based on HA-binding and hydrolysis data. HA sugar residues are drawn according to commonly accepted graphical carbohydrate symbolism (49); N-acetyl-D-glucosamine is depicted as a black square with black lines and D-glucuronic acid as a diamond with grey upper segment and black outline. Reducing ends of the substrate are indicated by R, non-reducing ends by N; in hydrolysis products R' and N' is used accordingly.

TABLE 1: **Kinetic parameters of HA-binding determined by QCM approach**

The kinetic data was evaluated using a two-state (sequential two-site) model and the kinetic parameters (mean ± SE) were calculated based on the average molecular mass of 750 kDa for HA.

| | INTERACTION PHASE | KINETIC PARAMETER | | HA concentration (mg/ml) 0.05 | 0.1 | 0.2 | 0.5 | 1.0 |
|---|---|---|---|---|---|---|---|---|
| NQ-BVH$^{WT}$ | EQUILIBRIUM | $K_{D1}$ (x $10^{-8}$) | (M) | 3.22 ± 0.12 | 3.05 ± 0.32 | 2.48 ± 0.16 | 9.84 ± 0.61 | 87.7 ± 2.76 |
| | | $K_{D2}$ (x $10^{-2}$) | | 5.48 ± 1.13 | 12.0 ± 3.70 | 52.0 ± 8.71 | 64.0 ± 17.6 | 0.69 ± 0.35 |
| | | $K_{DSUM}$ (x $10^{-9}$) | | 1.77 ± 0.43 | 3.66 ± 1.51 | 12.9 ± 3.00 | 62.9 ± 21.1 | 6.10 ± 3.26 |
| | ASSOCIATION | $k_{ass1}$ (x $10^{4}$) | ($M^{-1}\cdot s^{-1}$) | 66.7 ± 1.52 | 99.2 ± 4.72 | 106 ± 2.69 | 18.5 ± 0.39 | 3.34 ± 0.04 |
| | | $k_{ass2}$ (x $10^{-3}$) | | 54.9 ± 4.95 | 13.5 ± 1.89 | 2.64 ± 0.24 | 0.78 ± 0.14 | 8.62 ± 0.31 |
| | | $k_{assSUM}$ (x $10^{3}$) | | 36.6 ± 4.14 | 13.4 ± 2.51 | 2.80 ± 0.33 | 0.14 ± 0.03 | 0.29 ± 0.01 |
| | DISSOCIATION | $k_{diss1}$ (x $10^{-3}$) | ($s^{-1}$) | 21.5 ± 0.34 | 30.3 ± 1.72 | 26.3 ± 1.04 | 18.2 ± 0.74 | 29.3 ± 0.57 |
| | | $k_{diss2}$ (x $10^{-4}$) | | 30.1 ± 3.50 | 16.5 ± 2.78 | 13.7 ± 1.05 | 5.06 ± 0.48 | 0.00[(a)] ± 0.28 |
| | | $k_{dissSUM}$ (x $10^{-6}$) | | 64.7 ± 8.55 | 50.0 ± 11.3 | 36.0 ± 4.19 | 9.21 ± 1.25 | 1.76 ± 0.85 |
| NQ-BVH$^{\Delta L}$ | EQUILIBRIUM | $K_{D1}$ (x $10^{-8}$) | (M) | 2.40 ± 0.27 | 4.69 ± 0.49 | 2.59 ± 0.29 | 6.34 ± 0.55 | 12.5 ± 6.63 |
| | | $K_{D2}$ (x $10^{-2}$) | | 0.48 ± 0.09 | 0.91 ± 0.54 | 3.80 ± 1.03 | 1.11 ± 0.59 | 0.04 ± 0.03 |
| | | $K_{DSUM}$ (x $10^{-9}$) | | 0.11 ± 0.03 | 0.42 ± 0.29 | 0.98 ± 0.37 | 0.70 ± 0.44 | 0.05 ± 0.07 |
| | ASSOCIATION | $k_{ass1}$ (x $10^{4}$) | ($M^{-1}\cdot s^{-1}$) | 108 ± 9.06 | 78.3 ± 2.37 | 80.9 ± 2.55 | 37.3 ± 0.77 | 23.2 ± 10.3 |
| | | $k_{ass2}$ (x $10^{-3}$) | | 62.0 ± 2.02 | 42.4 ± 15.4 | 9.21 ± 0.58 | 5.41 ± 0.27 | 150 ± 30.9 |
| | | $k_{assSUM}$ (x $10^{3}$) | | 67.0 ± 7.80 | 33.2 ± 13.1 | 7.45 ± 0.70 | 2.01 ± 0.14 | 34.8 ± 22.6 |
| | DISSOCIATION | $k_{diss1}$ (x $10^{-3}$) | ($s^{-1}$) | 25.9 ± 0.69 | 36.7 ± 2.72 | 20.9 ± 1.65 | 23.6 ± 1.58 | 29.0 ± 2.51 |
| | | $k_{diss2}$ (x $10^{-4}$) | | 2.99 ± 0.48 | 3.84 ± 0.89 | 3.50 ± 0.73 | 0.00[(a)] ± 0.29 | 0.00[(a)] ± 0.37 |
| | | $k_{dissSUM}$ (x $10^{-6}$) | | 7.74 ± 1.45 | 14.1 ± 4.31 | 7.32 ± 2.10 | 1.42 ± 0.78 | 1.74± 1.22 |

(a) ClampXP2 cannot calculate $k_{diss}$ values under $10^{-4}$, therefore instead of zero, an estimated value, $0.6\cdot10^{-4}$ was substituted.

**Figure 1**

# A

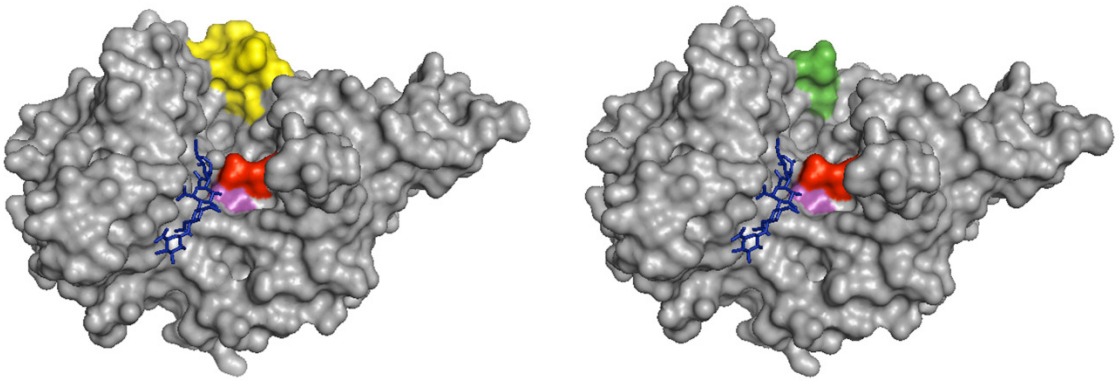
189 CYNLTPNQPSAQC 201
189 CGSGSC 194

# B

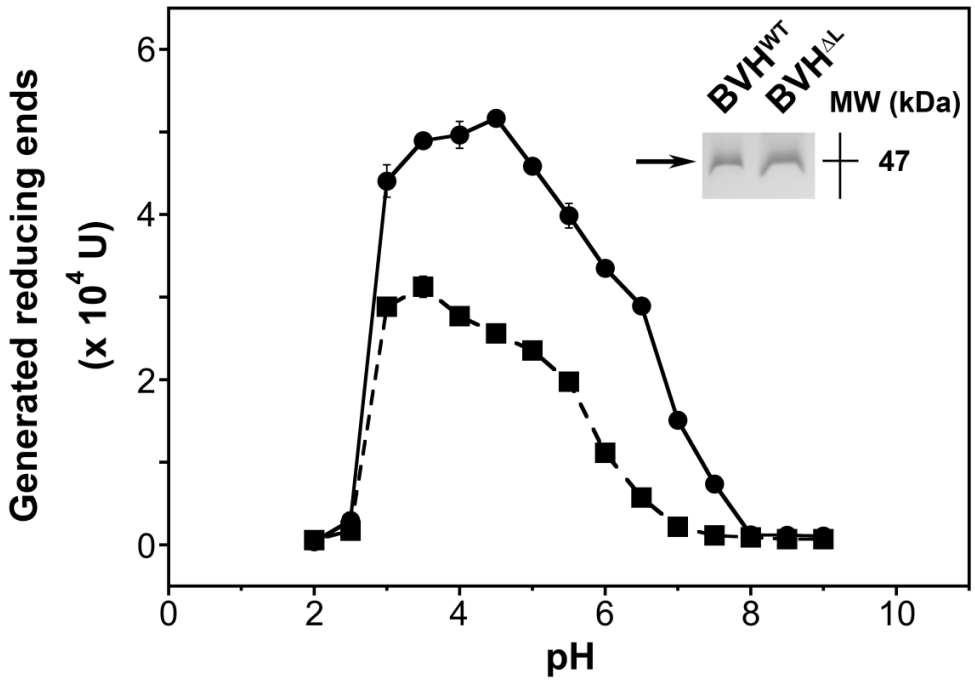
Generated reducing ends
(x 10^4 U)
pH
BVH^WT
BVH^ΔL
MW (kDa)
47
0
2
4
6
8
10

**Figure 2**

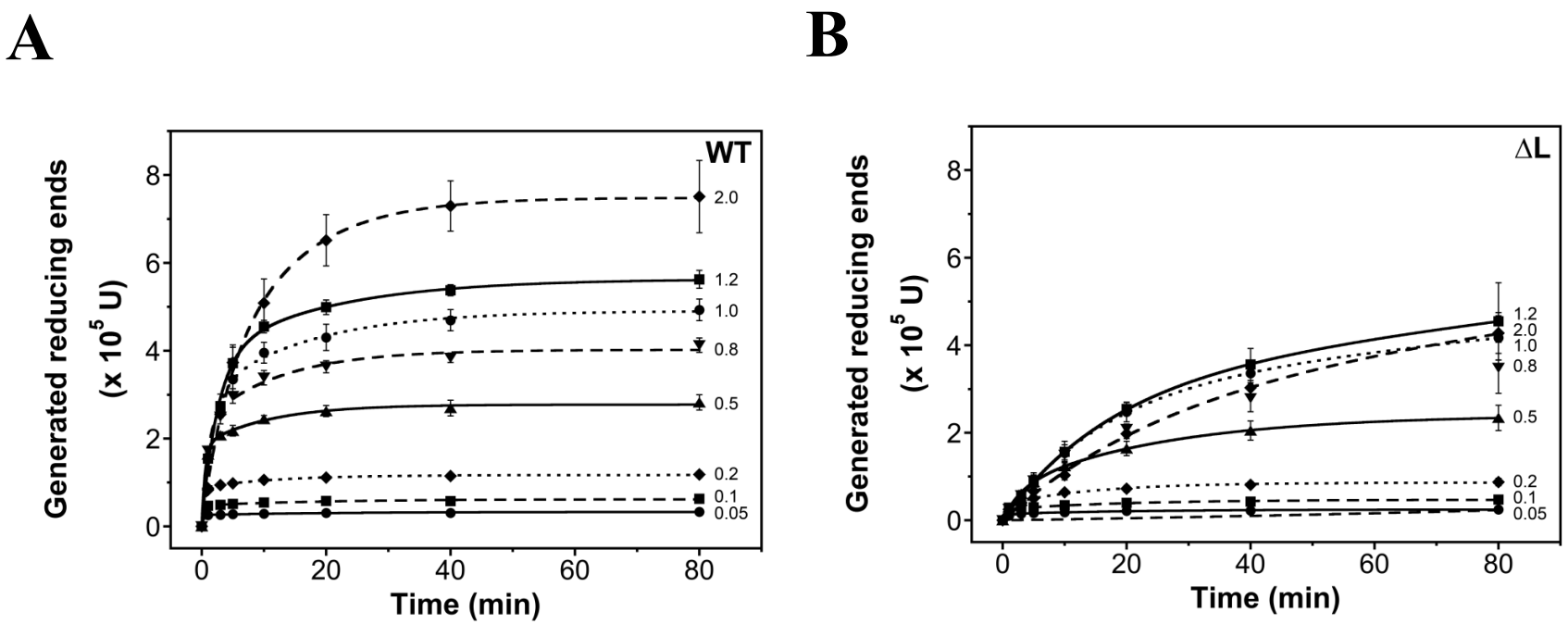
A
B
WT
ΔL
Generated reducing ends
(x 10^5 U)
Time (min)
2.0
1.2
1.0
0.8
0.5
0.2
0.1
0.05

**Figure 3**

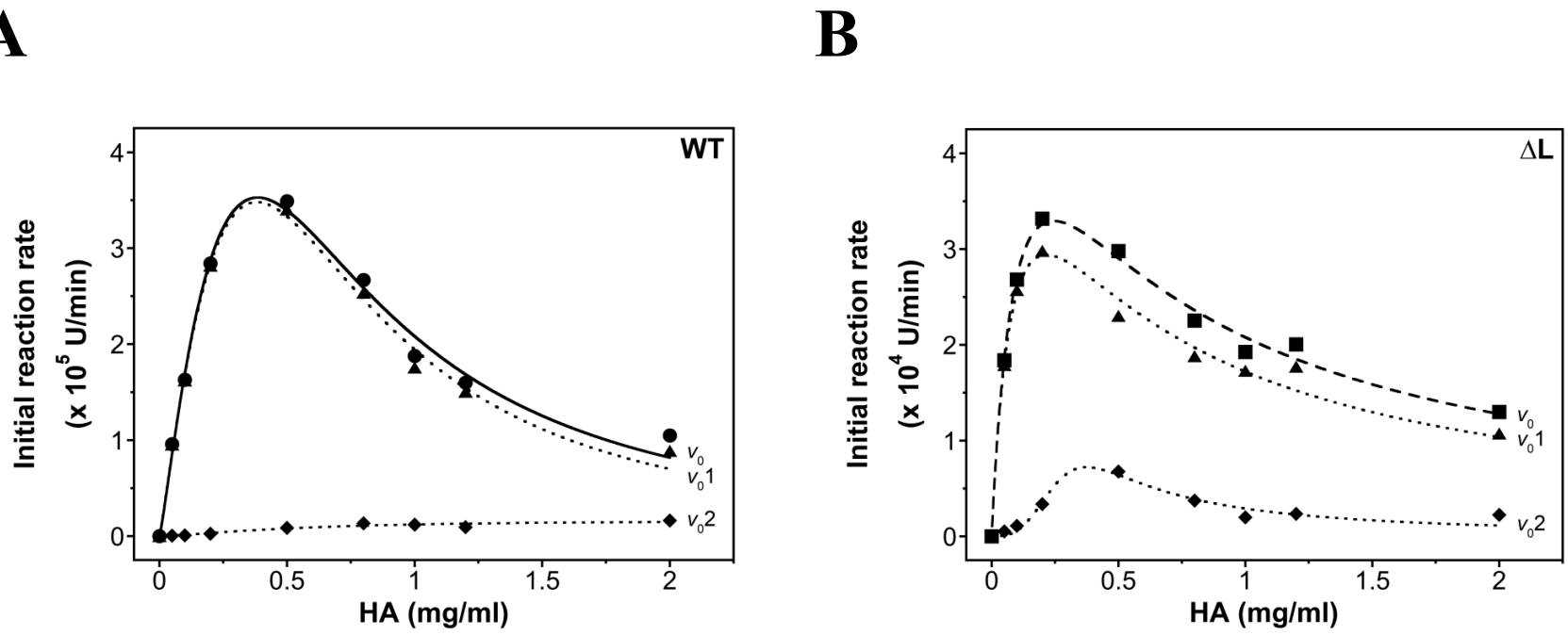
A
B
WT
ΔL
Initial reaction rate
(x 10^5 U/min)
(x 10^4 U/min)
HA (mg/ml)
v0
v0 1
v0 2

**Figure 4**

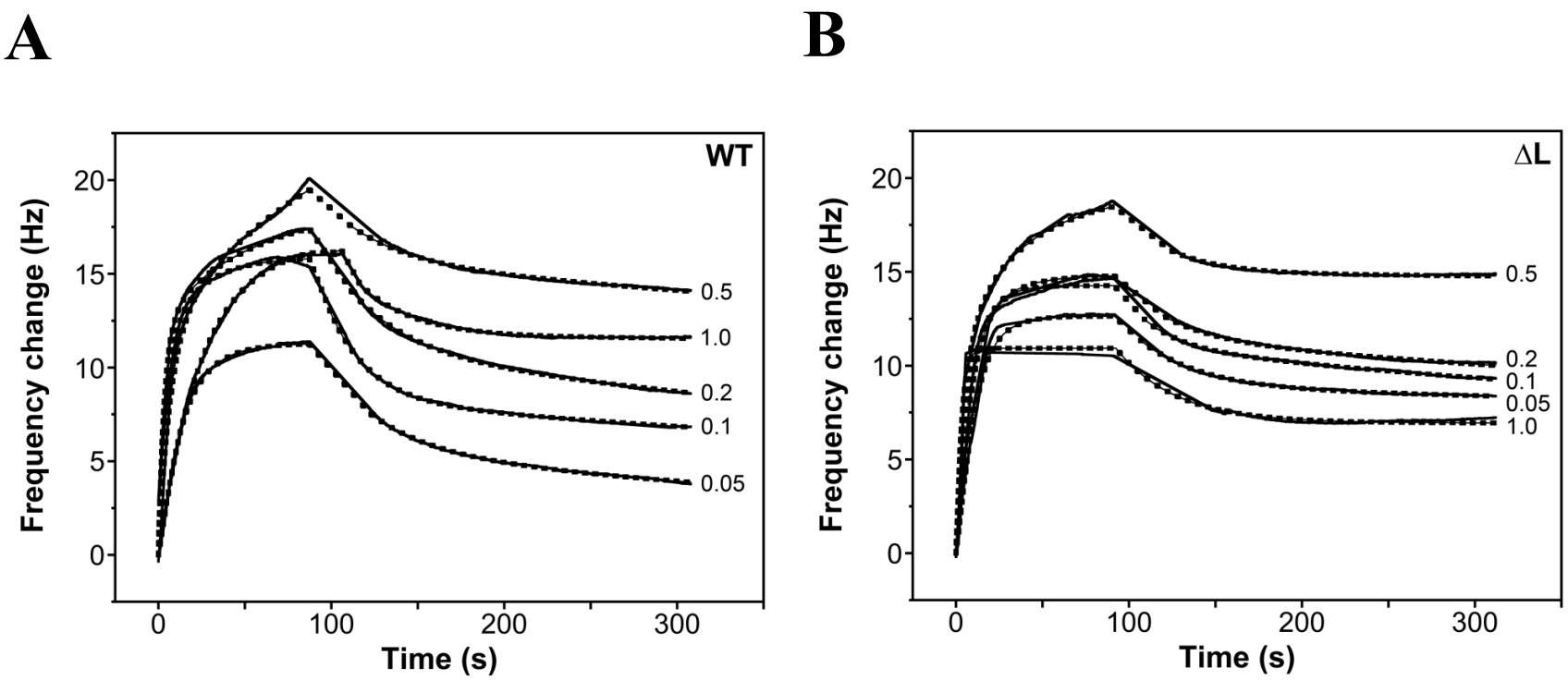
A
B
WT
ΔL
Frequency change (Hz)
Time (s)
0
5
10
15
20
0
100
200
300
0.5
1.0
0.2
0.1
0.05

**Figure 5**

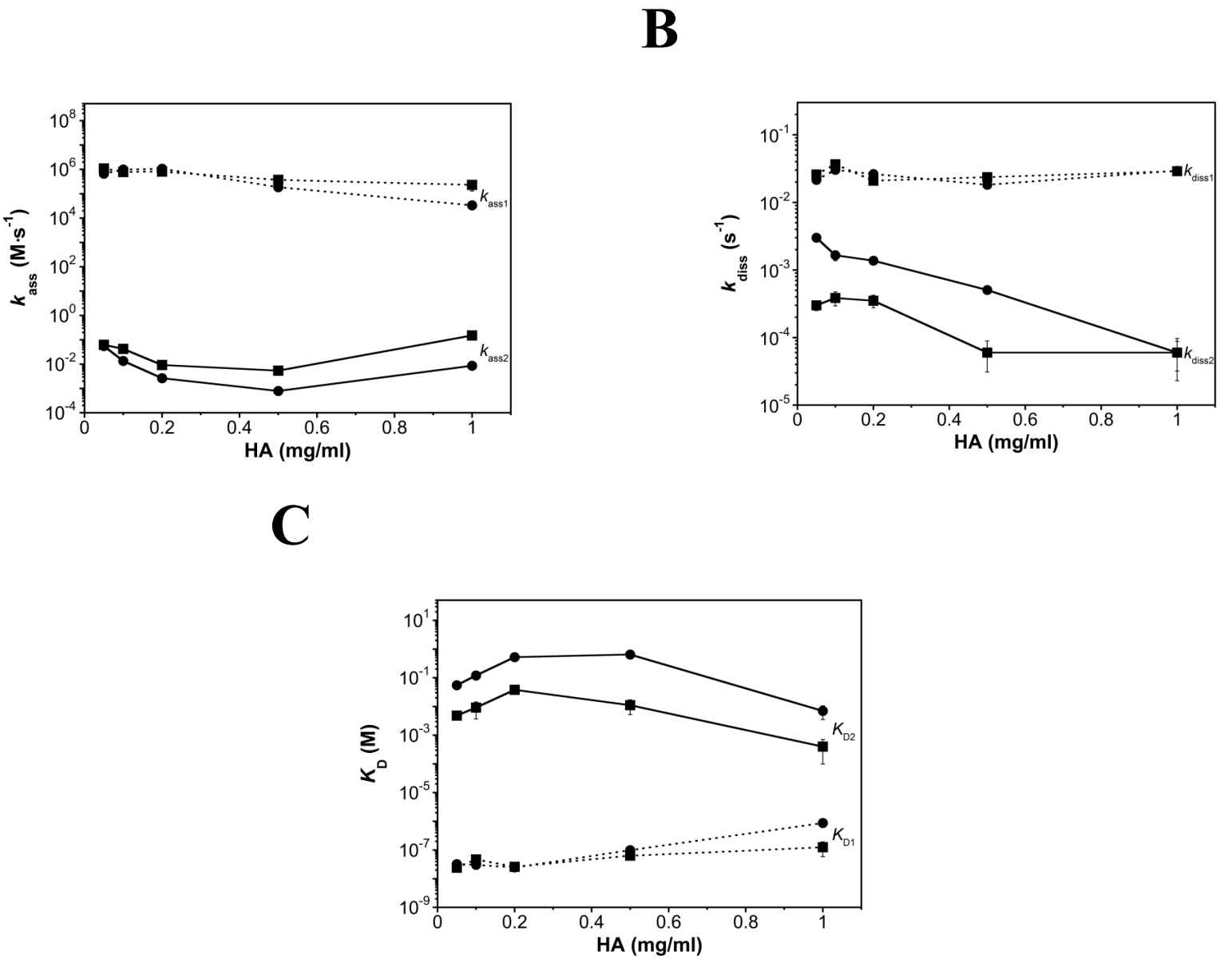
A
B
C
$k_{ass}$ ($M \cdot s^{-1}$)
$k_{ass1}$
$k_{ass2}$
HA (mg/ml)
$k_{diss}$ ($s^{-1}$)
$k_{diss1}$
$k_{diss2}$
HA (mg/ml)
$K_D$ (M)
$K_{D2}$
$K_{D1}$
HA (mg/ml)

**Figure 6**

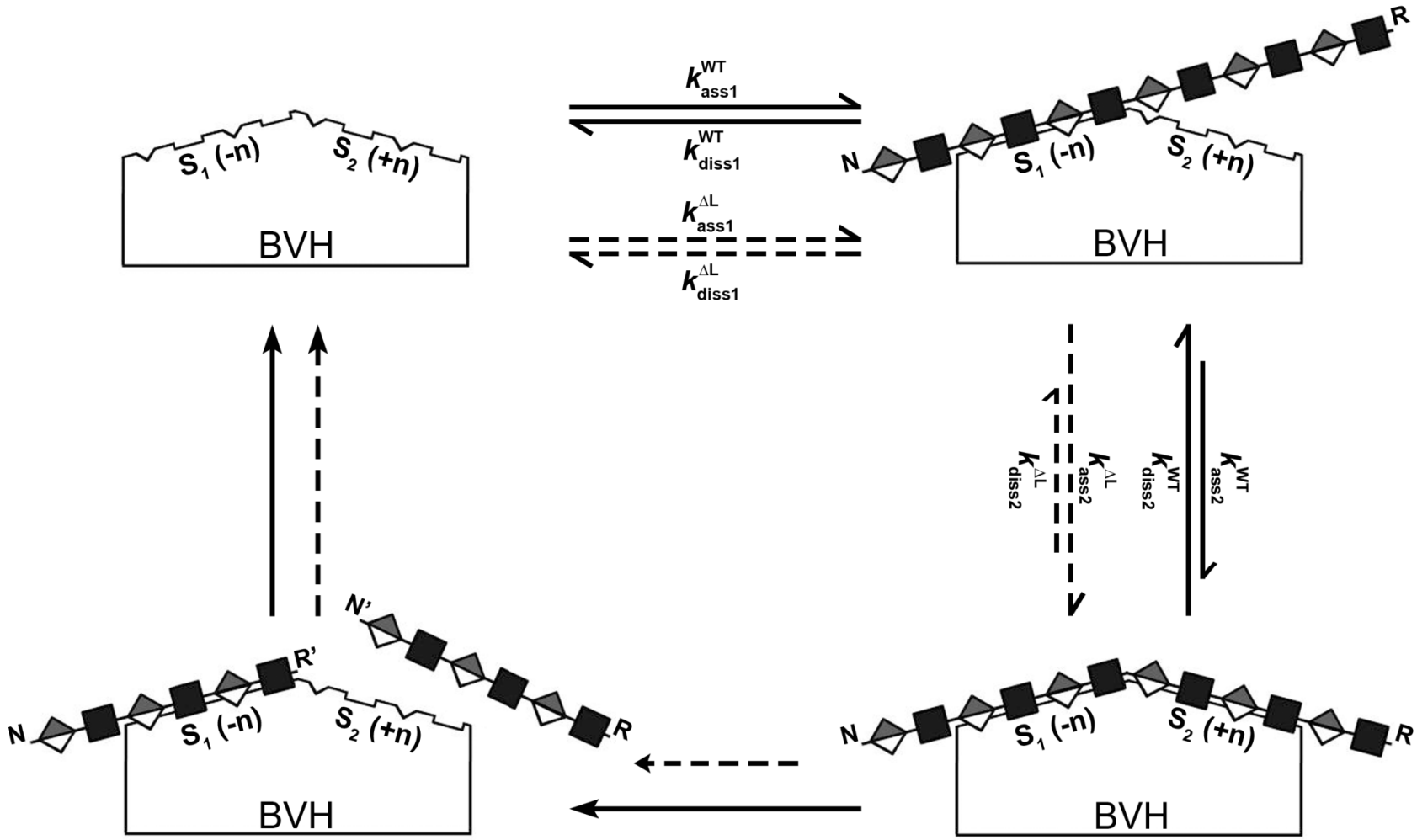
$k^{WT}_{ass1}$
$k^{WT}_{diss1}$
$k^{\Delta L}_{ass1}$
$k^{\Delta L}_{diss1}$
$k^{\Delta L}_{diss2}$
$k^{\Delta L}_{ass2}$
$k^{WT}_{diss2}$
$k^{WT}_{ass2}$
N
R
N'
R'
$S_1$ (-n)
$S_2$ (+n)
BVH